Effect of a side-connected dot in a T-shaped double quantum dot interferometer

2008 J. Phys.: Condens. Matter 20 195205

(http://iopscience.iop.org/0953-8984/20/19/195205)

J. Phys.: Condens. Matter **20** (2008) 195205 (11pp) doi:10.1088/0953-8984/20/19/195205

Effect of a side-connected dot in a T-shaped double quantum dot interferometer

Satoshi Kawaguchi

Department of Complex Systems, School of Systems Information Science,
Future University-Hakodate, Hakodate 041-8655, Japan

Received 3 December 2007, in final form 13 March 2008
Published 8 April 2008
Online at stacks.iop.org/JPhysCM/20/195205

Abstract

In this study we discuss the effect of a side-connected dot in a T-shaped double quantum dot (DQD) system under an infinitely large Coulomb interaction.

Applying the non-crossing approximation scheme to a T-shaped DQD interferometer, the effect of a side-connected dot on the Aharonov–Bohm (AB) oscillation is discussed. The AB oscillation in zero-bias conductance becomes large at an optimal interdot coupling. Under a finite bias voltage, the AB phase symmetry is broken in the transmission probability and differential conductance. The Fano interference depends on direct tunneling, temperature, and interdot coupling, and the amplitude of the AB oscillation is affected by these factors.

1. Introduction

Recent developments in the method of fabrication of nanoscale devices have opened up new areas of research in physics and information science. Scientists from different fields have devoted themselves to the study of nanostructures. Quantum dot systems exhibit interesting electron transport phenomena such as resonant tunneling, Coulomb blockade, and the Kondo effect [1–5]. In such nanodevices, the capacitance is so small that the charging energy becomes larger by a single electron. Then the Coulomb blockade and Kondo effect play important roles in electron conduction. In a quantum dot system, the number of electrons in the dot is very important. When the occupation number is even the spins of the electrons cancel each other. However, when the occupation number is odd an unpaired spin remains in the dot and the dot acts as a localized magnetic impurity. At low temperatures the exchange interaction between the electrons in the leads and the dot becomes strong. Then the spin in the dot couples with that of the conduction electrons in the leads to form a spin singlet state (Kondo singlet state). This causes a Kondo peak around the Fermi level in the density of states (DOS), and electron conduction takes place through resonant tunneling [6, 7].

There are three types of double quantum dot (DQD) system: serial, T-shaped, and parallel. They are classified by the coupling between the dots and leads. The geometry of DQD systems is shown in figure 1. In DQD systems, the interdot coupling significantly affects the electron conduction.

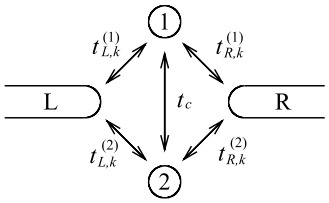

Figure 1. Double quantum dot (DQD) systems. For a serial DQD system, $t^{(1)}_{\mathrm{R},k} = t^{(2)}_{\mathrm{L},k} = 0$; for a T-shaped DQD system, $t^{(2)}_{\mathrm{L},k} = t^{(2)}_{\mathrm{R},k} = 0$; and for a parallel DQD, $t^{(1,2)}_{\mathrm{L,R},k} \neq 0$.

In serial DQD systems, formation of a local singlet state and the Kondo singlet state is competitive, causing the optimal interdot coupling for the conductance [8]. In T-shaped DQD systems, depending on the interdot coupling, the dependence of the conductance on temperature varies. In the case of large interdot coupling, the magnetic moments of the dots form a tightly bound singlet state, and the conductance decreases monotonically with temperature. However, in the case of small interdot coupling, the two-stage Kondo effect results in the non-monotonic dependence of the conductance on temperature and magnetic field. The optimal temperature and magnetic field for conductance appear due to the two-stage screening of the magnetic moment of the dots [9]. On the contrary, it is shown that the Kondo-mediated conductance is suppressed by a Fano-like effect when the interdot coupling is small and the energy levels of the dots are same [10].

An Aharonov–Bohm (AB) ring is used to measure the coherence of the electron conduction between two paths. A quantum dot embedded in one of the arms of the AB ring has been studied [11–15]. In this device, the differential conductance is modified by the magnetic flux penetrating the ring. The differential conductance is asymmetric with a dip and a peak, which is called the Fano resonance. The Fano resonance in the AB ring with one embedded dot is observed experimentally [16, 17]. This reflects the interference between the discrete energy levels of the dot and the continuum states of the ring. The electron tunneling in an AB interferometer with a single quantum dot and DQDs has been studied for the case of strong electron correlation [7, 18]. At high temperatures, the electrons tunneling via a dot are scattered by a local spin in the dot. With a decrease in the temperature, the spins in the dot and leads form the Kondo singlet state. As a spin in the dot is quenched, the electron conduction via the dot becomes coherent. Then the direct tunneling path between the leads and the path via the dot interfere strongly, and the AB oscillation becomes large. In addition, at low temperatures, the AB oscillation has higher harmonic components as the potentials of the dots deepen.

Although several studies have been carried out on AB interferometers with double dots in parallel configuration, no study has been carried out on T-shaped DQD interferometers. Unlike an AB interferometer with a single dot, it is expected that the interdot coupling causes unique variations in the conductance under strong electron correlation. In this study, we first consider a T-shaped DQD system under infinitely large Coulomb interaction in the dots. We formulate the non-crossing approximation (NCA) for the system in a non-equilibrium state. The dependence of the differential conductance on the interdot coupling, temperature, and energy levels of dots is examined. Next, we apply the NCA scheme to a T-shaped DQD interferometer. We study the effect of a side-connected dot on the conductance, and discuss the effect of direct tunneling, temperature, and interdot coupling on the AB oscillation.

2. Model Hamiltonian in the limit $U \to \infty$

We discuss the case for which the Coulomb interaction in the dots is infinitely large. We first formulate the NCA scheme by following the NCA schemes proposed by Pruschke and Grewe, and Hettler *et al* [19, 20]. Their methods are combined to study the DQD systems in non-equilibrium states. Although we derive the NCA formulation for general DQD systems, we analyze a T-shaped DQD system in the numerical calculation.

2.1. DQD systems in the absence of a magnetic field

Here, we consider DQD systems in the absence of a magnetic field. The geometry of the systems is shown in figure 1. In the NCA formalism, the total Hamiltonian of the system is written as

$$H_{\rm total} = H_{\rm loc} + H_{\rm med}, \tag{2.1}$$

where

$$\begin{aligned} H_{\rm loc} = &\sum_{\sigma}(\epsilon_1 d^{\dagger}_{1,\sigma} d_{1,\sigma} + \epsilon_2 d^{\dagger}_{2,\sigma} d_{2,\sigma}) \\ &+ \sum_{\sigma}(t_{\rm c} d^{\dagger}_{1,\sigma} d_{2,\sigma} + {\rm H.c.}) \\ &+ U(n_{1,+}n_{1,-} + n_{2,+}n_{2,-}) \end{aligned} \tag{2.2}$$

and

$$\begin{aligned} H_{\rm med} = &\sum_{k,\sigma}\epsilon_k c^{\dagger}_{{\rm L},k,\sigma} c_{{\rm L},k,\sigma} + \sum_{k,\sigma}\epsilon_k c^{\dagger}_{{\rm R},k,\sigma} c_{{\rm R},k,\sigma} \\ &+ \sum_{k,\sigma}(t^{(1)}_{{\rm L},k} c^{\dagger}_{{\rm L},k,\sigma} d_{1,\sigma} + t^{(2)}_{{\rm L},k} c^{\dagger}_{{\rm L},k,\sigma} d_{2,\sigma} + {\rm H.c.}) \\ &+ \sum_{k,\sigma}(t^{(1)}_{{\rm R},k} c^{\dagger}_{{\rm R},k,\sigma} d_{1,\sigma} + t^{(2)}_{{\rm R},k} c^{\dagger}_{{\rm R},k,\sigma} d_{2,\sigma} + {\rm H.c.}). \end{aligned} \tag{2.3}$$

Here, $H_{\rm loc}$ and $H_{\rm med}$ are the local and medium Hamiltonians, respectively, H.c. indicates the Hermitian conjugate, and σ ($= \pm$) represents the spin (up and down, respectively). $c^{\dagger}_{{\rm L(R)},k,\sigma}$ and $c_{{\rm L(R)},k,\sigma}$ represent the creation and annihilation operators, respectively, of an electron with momentum k and spin σ in the left (right) lead. $d_{1(2),\sigma}$ is the annihilation operator of an electron with spin σ in dot 1(2). Dot 1 is connected to the left and right leads with the tunneling amplitudes $t^{(1)}_{{\rm L},k}$ and $t^{(1)}_{{\rm R},k}$, respectively. Similar notation is used for dot 2. $t_{\rm c}$ indicates the interdot coupling and U indicates the Coulomb interaction. The number of electrons in dot i ($i = 1$ and 2) is defined as

$$n_{i,\sigma} = d^{\dagger}_{i,\sigma} d_{i,\sigma}. \tag{2.4}$$

In the limit $U \to \infty$, double occupancy of electrons in a dot is not allowed. Then, there are nine states of localized electrons in dots 1 and 2 [10]. It is necessary to diagonalize $H_{\rm loc}$ by using these base states. We introduce the Hubbard operator $X_{mn} = |m\rangle\langle n|$. Then, $H_{\rm loc}$ is written as

$$H_{\rm loc} = \sum_{m=1}^{9} E_m X_{mm}, \tag{2.5}$$

where E_m and $|m\rangle$ ($m = 1, 2, \ldots, 9$) are the eigenenergy and the corresponding eigenstate, respectively. Using the eigenstate, the fermionic annihilation operator is written as

$$d_{i,\sigma} = \sum_{n,m} U^{i\sigma}_{nm} X_{nm}, \tag{2.6}$$

where we have defined

$$U^{i\sigma}_{nm} = \langle n|d_{i,\sigma}|m\rangle. \tag{2.7}$$

Then, $H_{\rm med}$ can be written using the Hubbard operator as

$$\begin{aligned} H_{\rm med} = &\sum_{k,\sigma}\epsilon_k c^{\dagger}_{{\rm L},k,\sigma} c_{{\rm L},k,\sigma} + \sum_{k,\sigma}\epsilon_k c^{\dagger}_{{\rm R},k,\sigma} c_{{\rm R},k,\sigma} \\ &+ \sum_{k,\sigma}\sum_{n,m}(t^{(1)}_{{\rm L},k} U^{1\sigma}_{nm} c^{\dagger}_{{\rm L},k,\sigma} X_{nm} \\ &+ t^{(2)}_{{\rm L},k} U^{2\sigma}_{nm} c^{\dagger}_{{\rm L},k,\sigma} X_{nm} + {\rm H.c.}) \\ &+ \sum_{k,\sigma}\sum_{n,m}(t^{(1)}_{{\rm R},k} U^{1\sigma}_{nm} c^{\dagger}_{{\rm R},k,\sigma} X_{nm} \\ &+ t^{(2)}_{{\rm R},k} U^{2\sigma}_{nm} c^{\dagger}_{{\rm R},k,\sigma} X_{nm} + {\rm H.c.}). \end{aligned} \tag{2.8}$$

For each $|m\rangle$, the ionic resolvent and the corresponding local DOS are defined as

$$P_m^r(\omega) = \frac{1}{\omega - E_m - \Sigma_m^r(\omega)} \tag{2.9}$$

and

$$\rho_m(\omega) = -\frac{1}{\pi}\,\mathrm{Im}\,P_m^r(\omega), \tag{2.10}$$

respectively. The self-energy of $|m\rangle$ is given by

$$\begin{aligned}\Sigma_m^r(\omega) = &\sum_{n,\sigma}(|U_{nm}^{1\sigma}|^2 + |U_{mn}^{1\sigma}|^2)\left(\frac{1}{\pi}\right)\\ &\times\int_{-\infty}^{\infty}\mathrm{d}\epsilon\,[\Gamma_{11}^{\mathrm{L}}f(\epsilon-\mu_{\mathrm{L}}) + \Gamma_{11}^{\mathrm{R}}f(\epsilon-\mu_{\mathrm{R}})]P_n^r(\omega+\epsilon)\\ &+\sum_{n,\sigma}(|U_{nm}^{2\sigma}|^2 + |U_{mn}^{2\sigma}|^2)\left(\frac{1}{\pi}\right)\\ &\times\int_{-\infty}^{\infty}\mathrm{d}\epsilon\,[\Gamma_{22}^{\mathrm{L}}f(\epsilon-\mu_{\mathrm{L}}) + \Gamma_{22}^{\mathrm{R}}f(\epsilon-\mu_{\mathrm{R}})]P_n^r(\omega+\epsilon),\end{aligned} \tag{2.11}$$

where we have neglected the vertex corrections. The linewidth functions are

$$\Gamma_{ij}^{\mu}(\epsilon) = 2\pi\sum_k t_{\mu,k}^{(i)*}t_{\mu,k}^{(j)}\delta(\epsilon-\epsilon_k). \tag{2.12}$$

In this study, we assume that the DOS of the leads is constant under a wide band limit. Then, $\Gamma_{ij}^{\mu}(\epsilon)$ is a constant independent of ϵ. $f(\omega)$ is the Fermi distribution function, $f(\omega) = \frac{1}{\mathrm{e}^{\beta\omega}+1}$ with $\beta = 1/k_{\mathrm{B}}T$. In order to solve equation (2.11) self-consistently, we introduce a new variable:

$$A_m(\omega) = -\frac{1}{\pi}\,\mathrm{Im}\,P_m^r(\omega) = -\frac{1}{\pi}\,\mathrm{Im}\,\Sigma_m^r(\omega)|P_m^r(\omega)|^2. \tag{2.13}$$

Using this variable, equation (2.11) can be written as

$$\begin{aligned}\frac{A_m(\omega)}{|P_m^r(\omega)|^2} = &\sum_{n,\sigma}(|U_{nm}^{1\sigma}|^2 + |U_{mn}^{1\sigma}|^2)\left(\frac{1}{\pi}\right)\\ &\times\int_{-\infty}^{\infty}\mathrm{d}\epsilon\,[\Gamma_{11}^{\mathrm{L}}f(\epsilon-\mu_{\mathrm{L}}) + \Gamma_{11}^{\mathrm{R}}f(\epsilon-\mu_{\mathrm{R}})]A_n(\omega+\epsilon)\\ &+\sum_{n,\sigma}(|U_{nm}^{2\sigma}|^2 + |U_{mn}^{2\sigma}|^2)\left(\frac{1}{\pi}\right)\\ &\times\int_{-\infty}^{\infty}\mathrm{d}\epsilon\,[\Gamma_{22}^{\mathrm{L}}f(\epsilon-\mu_{\mathrm{L}}) + \Gamma_{22}^{\mathrm{R}}f(\epsilon-\mu_{\mathrm{R}})]A_n(\omega+\epsilon).\end{aligned} \tag{2.14}$$

The real part of $\Sigma_m^r(\omega)$ is obtained by the Kramers–Kronig relation,

$$\mathrm{Re}\,\Sigma_m^r(\omega) = \frac{1}{\pi}\mathrm{P}\int\mathrm{d}\epsilon\,\frac{\mathrm{Im}\,\Sigma_m^r(\epsilon)}{\epsilon-\omega}, \tag{2.15}$$

where P denotes the Cauchy principal part. The definition of the Green's function between dots i and j is (sub-indices are omitted here)

$$G_{ij,\sigma}(t,t') = -\mathrm{i}\langle\mathrm{T_C}\{d_{i,\sigma}(t)d_{j,\sigma}^{\dagger}(t')\}\rangle, \tag{2.16}$$

where $\mathrm{T_C}$ is the time-ordering operator along the Keldysh contour C, which consists of the forward C_- and the backward C_+ paths. Applying the usual NCA scheme, we can obtain the retarded Green's function as

$$G_{ij,\sigma}^r(\omega) = \sum_{n,m}U_{nm}^{i\sigma}U_{nm}^{j\sigma}\langle\langle X_{nm};X_{mn}\rangle\rangle_{\omega}, \tag{2.17}$$

where

$$\begin{aligned}\langle\langle X_{nm};X_{mn}\rangle\rangle_{\omega} = &\frac{1}{Z_{\mathrm{loc}}}\int_{-\infty}^{\infty}\mathrm{d}\epsilon\,\mathrm{e}^{-\beta\epsilon}[\rho_n(\epsilon)P_m^r(\epsilon+\omega)\\ &-\rho_m(\epsilon)P_n^r(\epsilon-\omega)].\end{aligned} \tag{2.18}$$

Here, the partition function

$$Z_{\mathrm{loc}} = \sum_{m=1}^{9}\int_{-\infty}^{\infty}\mathrm{d}\epsilon\,\mathrm{e}^{-\beta\epsilon}\rho_m(\epsilon). \tag{2.19}$$

The spectral function between dots i and j is given by

$$A_{ij,\sigma}^{(d)}(\omega) = -\frac{1}{\pi}\,\mathrm{Im}\,G_{ij,\sigma}^r(\omega). \tag{2.20}$$

In order to absorb the Boltzmann factor in the integrals of equations (2.18) and (2.19), we introduce a new quantity given as

$$a_m(\omega) = \mathrm{e}^{-\beta\omega}\rho_m(\omega) = \mathrm{e}^{-\beta\omega}A_m(\omega) = \frac{\mathrm{i}}{2\pi}G_m^{<}(\omega), \tag{2.21}$$

where $G_m^{<}(\omega)$ is the Fourier transform of the lesser Green's function used in the Keldysh formalism. From equation (2.14), $a_m(\omega)$ satisfies

$$\begin{aligned}\frac{a_m(\omega)}{|P_m^r(\omega)|^2} = &\sum_{n,\sigma}(|U_{nm}^{1\sigma}|^2 + |U_{mn}^{1\sigma}|^2)\left(\frac{1}{\pi}\right)\\ &\times\int_{-\infty}^{\infty}\mathrm{d}\epsilon\,[\Gamma_{11}^{\mathrm{L}}f(\mu_{\mathrm{L}}-\epsilon) + \Gamma_{11}^{\mathrm{R}}f(\mu_{\mathrm{R}}-\epsilon)]a_n(\omega+\epsilon)\\ &+\sum_{n,\sigma}(|U_{nm}^{2\sigma}|^2 + |U_{mn}^{2\sigma}|^2)\left(\frac{1}{\pi}\right)\\ &\times\int_{-\infty}^{\infty}\mathrm{d}\epsilon\,[\Gamma_{22}^{\mathrm{L}}f(\mu_{\mathrm{L}}-\epsilon) + \Gamma_{22}^{\mathrm{R}}f(\mu_{\mathrm{R}}-\epsilon)]a_n(\omega+\epsilon).\end{aligned} \tag{2.22}$$

Finally, it is necessary to solve equations (2.14) and (2.22) self-consistently. Using A_m and a_m, equations (2.19) and (2.20) can be rewritten as

$$Z_{\mathrm{loc}} = \sum_{m=1}^{9}\int_{-\infty}^{\infty}\mathrm{d}\epsilon\,a_m(\epsilon) \tag{2.23}$$

and

$$\begin{aligned}A_{ij,\sigma}^{(d)}(\omega) = &\frac{1}{Z_{\mathrm{loc}}}\sum_{n,m}U_{nm}^{i\sigma}U_{nm}^{j\sigma}\\ &\times\int_{-\infty}^{\infty}\mathrm{d}\epsilon\,[a_n(\epsilon)A_m(\epsilon+\omega) - a_m(\epsilon)A_n(\epsilon-\omega)],\end{aligned} \tag{2.24}$$

respectively. The real part of $G_{ij,\sigma}^r$ is obtained by using the Kramers–Kronig relation as

$$\mathrm{Re}\,G_{ij,\sigma}^r(\omega) = \frac{1}{\pi}\mathrm{P}\int\mathrm{d}\epsilon\,\frac{\mathrm{Im}\,G_{ij,\sigma}^r(\epsilon)}{\epsilon-\omega}. \tag{2.25}$$

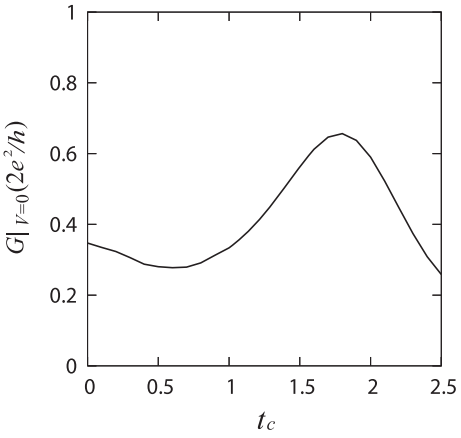

Figure 2. Dependence of zero-bias conductance on t_c. $k_BT = 0.05$, $\epsilon_1 = -2.0$, and $\epsilon_2 = -3.0$.

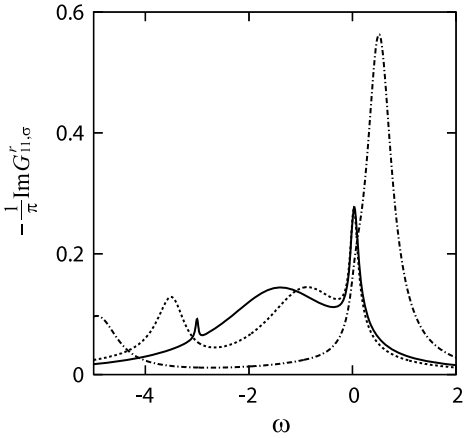

Figure 3. Density of states of dot 1 under zero-bias voltage. $k_BT = 0.05$, $\epsilon_1 = -2.0$, and $\epsilon_2 = -3.0$. Solid, dotted, and dash–dot curves represent cases $t_c = 0.1$, 1.0, and 2.5, respectively.

The lesser Green's function $G^<_{ij,\sigma}$ is obtained as

$$G^<_{ij,\sigma}(\omega) = \frac{1}{Z_{\rm loc}} \mathrm{i} \sum_{n,m} U^{i\sigma}_{nm} U^{j\sigma}_{nm} \int \mathrm{d}\epsilon\, a_n(\epsilon) A_m(\epsilon - \omega). \tag{2.26}$$

The NCA conserves current, and the average current satisfies $I = I_{\rm L} = -I_{\rm R}$. The current under the bias voltage is obtained by using the equation of motion method [21]. Using the matrix notation of G and Γ, the average current is written as

$$\begin{aligned} I &= \left(\frac{I_{\rm L} - I_{\rm R}}{2}\right) = \frac{e}{h} \sum_\sigma \mathrm{Re} \int \mathrm{Tr}\Big[\frac{\mathrm{i}}{2}(\mathbf{\Gamma}^{\rm L} - \mathbf{\Gamma}^{\rm R})\mathbf{G}^<_\sigma \\ &\quad + \mathrm{i}(f_{\rm L}\mathbf{\Gamma}^{\rm L} - f_{\rm R}\mathbf{\Gamma}^{\rm R})\mathbf{G}^r_\sigma\Big]\,\mathrm{d}\omega \\ &= \frac{\mathrm{i}e}{2h} \sum_\sigma \int \mathrm{Tr}[(\mathbf{\Gamma}^{\rm L} - \mathbf{\Gamma}^{\rm R})\mathbf{G}^<_\sigma \\ &\quad + (f_{\rm L}\mathbf{\Gamma}^{\rm L} - f_{\rm R}\mathbf{\Gamma}^{\rm R})(\mathbf{G}^r_\sigma - \mathbf{G}^a_\sigma)]\,\mathrm{d}\omega, \end{aligned} \tag{2.27}$$

where we have defined

$$\mathbf{\Gamma}^\mu = \begin{pmatrix} \Gamma^\mu_{11} & \Gamma^\mu_{12} \\ \Gamma^\mu_{21} & \Gamma^\mu_{22} \end{pmatrix} \tag{2.28}$$

and

$$\mathbf{G}^\nu_\sigma = \begin{pmatrix} G^\nu_{11,\sigma} & G^\nu_{12,\sigma} \\ G^\nu_{21,\sigma} & G^\nu_{22,\sigma} \end{pmatrix}. \tag{2.29}$$

Here, $\mu = \mathrm{L}, \mathrm{R}$, and $\nu = <, r, a$ [22]. The Fermi distribution functions of the left and right leads are defined as $f_{\rm L(R)}(\omega) = \frac{1}{\mathrm{e}^{\beta(\omega - \mu_{\rm L(R)})}+1}$. The differential conductance $(\mathrm{d}I/\mathrm{d}V)$ is obtained by the numerical derivative of the current equation, equation (2.27). Thus, we have formulated the NCA scheme for a DQD system under bias voltage. It should be noted that the vertex correction plays an important role in quantum coherence in serial DQD systems [23]. However, as far as the one-particle spectral function is concerned, the vertex correction is not so important. In T-shaped DQD systems, it is expected that we can omit the vertex correction [10].

For the T-shaped DQD system, we choose the elements of $\mathbf{\Gamma}$ such that $\Gamma^{\rm L}_{11} = \Gamma^{\rm R}_{11} = \Gamma$, and other elements are set to zero. $\Gamma = 1.0$ is fixed, and all energies are scaled by Γ. The values of t_c, eV, and k_BT are changed, and the dependence of the conductance on these variables is studied. The bias voltage is supplied symmetrically such that $\mu_{\rm L} = -\mu_{\rm R} = eV/2$. We choose the bare energy levels as $\epsilon_1 = -2.0$ and $\epsilon_2 = -3.0$. For these parameters, $n_1 \sim n_2 \sim 1.0$ under the zero-bias voltage, and the system is in the Kondo region.

The Kondo temperature $T^0_{\rm K}$ for a single dot in the limit $U \to \infty$ is $T^0_{\rm K} \sim D\sqrt{\Gamma/\pi|\epsilon_0|}\exp[-\pi|\epsilon_0|/\Gamma]$. For the parameters $D = 10.0$ and $\epsilon_0/\Gamma = -2.0$, $T^0_{\rm K} \sim 1.0 \times 10^{-2}$. For DQD systems, the effective Kondo temperature becomes exponentially large as $T_{\rm K} \sim T^0_{\rm K}\exp[(\frac{t_c}{\Gamma})\tan^{-1}(\frac{t_c}{\Gamma})]$ [24]. For the present parameters, the effective Kondo temperature is $T_{\rm K} \sim 1.0 \times 10^{-1}$. It is known that the NCA results obtained at low temperatures are not reliable [6]. Thus, we analyze the temperature region for which $k_BT \geqslant 0.05$. We choose such that the Fermi energy level is at the origin, $\omega = 0$.

The dependence of the zero-bias conductance at $k_BT = 0.05$ on t_c is shown in figure 2. We observe that there is an optimal t_c. In DQD systems, when $U \gg t_c$, the interdot coupling causes the effective antiferromagnetic coupling $J = t_c^2/U$ [8, 25]. Although $J \to 0$ in the limit $U \to \infty$, it is expected that the Kondo singlet state competes with the local singlet state. For a small t_c, a spin in dot 1 forms the Kondo singlet state with the conduction electrons in the leads, and the conductance becomes large. As t_c increases, the local spins in each dot form the spin singlet state. The formation of these two singlet states is competitive, and the formation of the spin singlet state leads to the decrease in the conductance. On the other hand, for a large t_c, the bare energy levels $\epsilon_{1,2}$ combine to form effective energy levels of the two dots, which are given by $\epsilon_\pm = \frac{1}{2}[(\epsilon_1 + \epsilon_2) \pm \sqrt{(\epsilon_1 - \epsilon_2)^2 + 4t_c^2}]$ [10]. As t_c increases, when ϵ_+ passes through the Fermi level, the DOS around the Fermi level becomes large, and the conductance is enhanced. However, for a significantly large t_c, ϵ_+ is located far away from the Fermi level, and the conductance reduces [26]. The above factors result in an optimal t_c.

The DOS of dot 1 under zero-bias voltage is shown in figure 3. It is observed that there is a sharp Kondo peak at

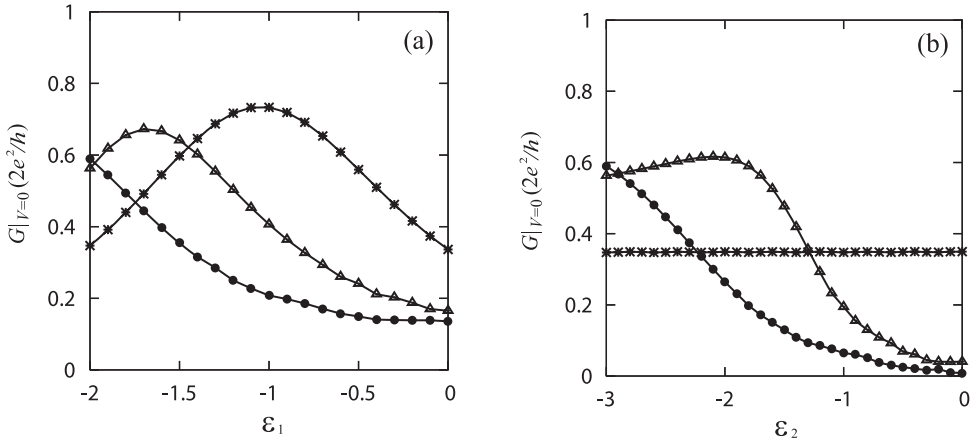

Figure 4. Dependence of zero-bias conductance on energy levels of dots. $k_BT = 0.05$. Curves denoted by $*$, $\triangle$, and $\bullet$ correspond to cases $t_c = 0.0$, 1.5, and 2.0, respectively. (a) $\epsilon_2 = -3.0$ and (b) $\epsilon_1 = -2.0$.

$\omega = 0$. Further, a small peak corresponding to the energy level of dot 2 is observed for a small t_c. With an increase in t_c, the width of this small peak increases and the peak shifts toward the lower energy. For a significantly large t_c, the bare energy levels combine, and the effective energy levels $\epsilon_\pm$ are formed. For a large t_c, although the Kondo peak exists around $\omega = 0$, it is not distinguishable because it is hindered by a large peak at the effective energy level ϵ_+. We can see that the large peak in the range $\omega > 0$ in the case of $t_c = 2.5$ corresponds to the effective energy level ϵ_+ and is not the Kondo peak. It is known that the splitting of the Coulomb peak indicates the coherence between single-particle states, and the gap of the splitting is given by $\Delta\epsilon_\pm = \sqrt{(\epsilon_1 - \epsilon_2)^2 + 4t_c^2}$ [27]. Although the Kondo peak also splits into bonding and antibonding combinations, its energy scale is significantly smaller than that of the Coulomb peak. The splitting of the Kondo peak indicates the quantum coherence between the two many-body Kondo states in each dot. In our calculation, only the splitting of the Coulomb peak is observed, which corresponds to the formation of the bonding and antibonding combinations of the single-particle levels $\epsilon_\pm$.

The dependence of the zero-bias conductance on the energy levels of the dots is shown in figure 4. For a fixed ϵ_2 with a large t_c, as $|\epsilon_1|$ increases, the effective energy level ϵ_+ shifts above the Fermi level. When ϵ_+ passes through the Fermi level, the zero-bias conductance becomes large. As a result, for a larger t_c, the optimal $|\epsilon_1|$, for which the zero-bias conductance has the maximum value, increases, as shown in figure 4(a). A similar behavior is observed for a fixed ϵ_1 with a large t_c.

The differential conductance for different values of t_c is shown in figure 5. The shape of the differential conductance depends on t_c. For a small t_c, the differential conductance has its maximum value at $V = 0$. As t_c increases, the zero-bias conductance increases and attains the maximum value for the optimal t_c. With further increase in t_c, the peak at $V = 0$ splits symmetrically and the differential conductance has two maximum values at $V \neq 0$. This behavior appears similar to the splitting of the zero-bias anomaly in serial DQD systems [28, 29]. It suggests that the formation of the quantum coherence of the two many-body Kondo states in each dot

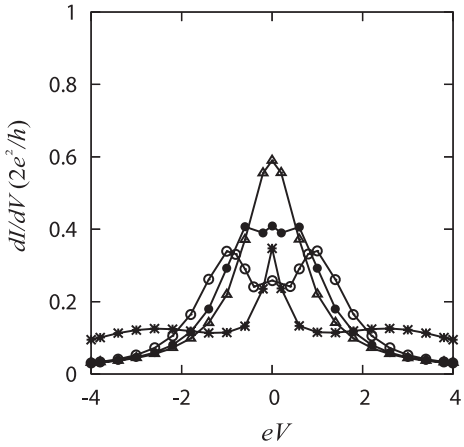

Figure 5. Differential conductance. $k_BT = 0.05$, $\epsilon_1 = -2.0$, and $\epsilon_2 = -3.0$. Curves denoted by $*$, $\triangle$, $\bullet$, and $\circ$ correspond to cases $t_c = 0.0$, 2.0, 2.25, and 2.5, respectively.

is caused by the interdot coupling. The quantum coherence occurs at temperatures that are significantly lower than those in our study; hence, the splitting in our calculation originates from a different mechanism. As shown in figure 2, there is an optimal $t_c(\sim 2.0)$ for the zero-bias conductance. For couplings larger than the optimal t_c, the energy levels of dots combine to form $\epsilon_\pm$. A large peak corresponding to ϵ_+, which is located above the Fermi level in the DOS, is observed. As ϵ_+ shifts away from the Fermi level, the zero-bias conductance decreases. On the contrary, the differential conductance at the finite voltage becomes large because the second term of equation (2.27) becomes large in the range $\omega > 0$.

The temperature dependence of the zero-bias conductance is shown in figure 6. For a small t_c, the zero-bias conductance increases monotonically with a decrease in the temperature. This property is similar to that of a single-dot system. At high temperatures, the Coulomb blockade suppresses the conductance. As the temperature decreases, the Kondo singlet state is formed between the electrons in the leads and dot 1, and the conductance is enhanced. With an increase in t_c ($\leqslant 2.0$), the zero-bias conductance becomes large at low temperatures.

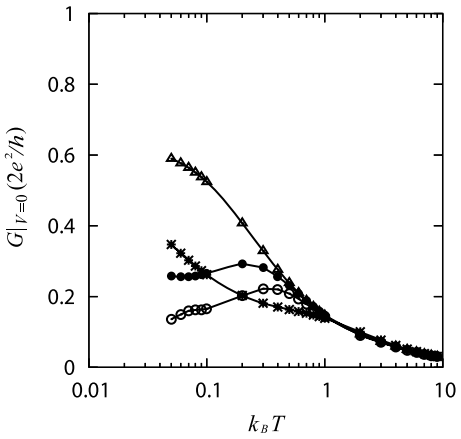

Figure 6. Dependence of zero-bias conductance on temperature. $\epsilon_1 = -2.0$, and $\epsilon_2 = -3.0$. Curves denoted by $*$, $\triangle$, $\bullet$, and $\circ$ correspond to cases $t_c = 0.0$, 2.0, 2.5, and 2.75, respectively.

However, for a significantly large t_c, the effective energy level ϵ_+ shifts above the Fermi level, and the DOS at the Fermi level reduces. At low temperatures, the integral value of the second term in equation (2.27) is small due to a small overlap of the two functions. As a result, the zero-bias conductance is strongly suppressed at low temperatures; however, at high temperatures, the integral value increases. As a result, there exists a local maximum zero-bias conductance at the optimal temperature.

Here, we present a brief conclusion for the T-shaped DQD system. Similar studies on T-shaped DQD systems have been carried out [1, 10], and the dependence of conductance on t_c, the energy levels of dots, and the DOS under zero-bias voltage have been studied. In this study, in addition to the above mentioned investigations, we have focused on the behavior of conductance under bias voltage at finite temperatures. We have shown that there exists an optimal t_c in the zero-bias conductance and studied the dependence of the DOS on t_c. These properties result in an optimal bias voltage for the differential conductance in case of a large t_c. The study of the temperature dependence of the zero-bias conductance has shown that there exists an optimal temperature for a large t_c.

In the following subsection, we study the properties of a T-shaped DQD interferometer taking into consideration the above mentioned results.

2.2. The AB effect in a T-shaped DQD interferometer

In this subsection we consider a T-shaped DQD system under a magnetic field. We apply the NCA scheme formulated in the previous subsection, and study the effect of a side-connected dot on the conductance. The geometry of the system is shown in figure 7: the loop made by the direct tunneling and the tunneling via dot 1 causes the AB effect in the current. The asymmetric coupling factor is defined as $\alpha = 4\Gamma^{\rm L}_{11}\Gamma^{\rm R}_{11}/(\Gamma^{\rm L}_{11} + \Gamma^{\rm R}_{11})^2$. We assume that the coupling between the leads and dot 1 is symmetric, i.e. $\alpha = 1.0$. The total linewidth function is $\Gamma = \Gamma^{\rm L}_{11} + \Gamma^{\rm R}_{11}$. Here, we neglect the Zeeman splitting of the energy levels.

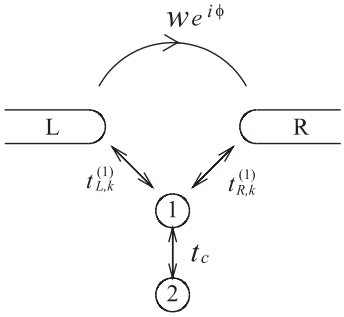

Figure 7. T-shaped DQD interferometer. $t^{(2)}_{{\rm L},k} = t^{(2)}_{{\rm R},k} = 0$.

Under the magnetic field, $H_{\rm AB}$ is introduced in addition to $H_{\rm total}$, which is given as

$$H_{\rm AB} = \sum_{k,k',\sigma} (W{\rm e}^{{\rm i}\phi} c^{\dagger}_{{\rm R},k,\sigma} c_{{\rm L},k',\sigma} + {\rm H.c.}). \tag{2.30}$$

The amplitude of the direct tunneling between the leads is given by $W{\rm e}^{{\rm i}\phi}$. The AB phase is given by $\phi = 2\pi\Phi/\Phi_0$, where Φ is the magnetic flux penetrating the ring and $\Phi_0 = \frac{hc}{e}$ is the flux quantum. As compared to the electrons passing via dot 1, the electrons passing directly between two leads have a phase difference of ϕ. The dimensionless measure of the direct tunneling between the leads is $\xi = (\pi\nu W)^2$, where ν is the DOS in the leads. We choose $\xi = 0.05$, unless otherwise stated. The transmission probability through a direct path is $T_r = 4\xi/(1+\xi)^2$.

For the case $t_c = 0$, the detailed derivation of current is provided in [11, 12]. Here, we explain the derivation briefly. The current from the left lead to dot 1, $I_{\rm L}$, is calculated by the time evolution of the occupation number $N_{\rm L} = \Sigma_{k,\sigma} c^{\dagger}_{{\rm L},k,\sigma} c_{{\rm L},k,\sigma}$. Using the equation of motion method with the Keldysh formalism [21], $I_{\rm L}$ is given by

$$I_{\rm L} = \frac{2e}{h} \sum_{\sigma} \int {\rm d}\omega \, {\rm Re} \Bigg[\sum_{k} t^{(1)}_{{\rm L},k} G^{<}_{1,{\rm L}k,\sigma}(\omega) + W{\rm e}^{-{\rm i}\phi} \sum_{k,k'} G^{<}_{{\rm R}k,{\rm L}k',\sigma}(\omega) \Bigg], \tag{2.31}$$

where $G^{<}_{1,{\rm L}k,\sigma}$, and $G^{<}_{{\rm R}k,{\rm L}k',\sigma}$ are the lesser Green's functions between the electrons in dot 1 and the left lead, and the electrons in the right and left leads, respectively. The current from the right lead to dot 1, $I_{\rm R}$, is obtained similarly. Using the Dyson equation and the analytic continuation rules, we calculate the non-equilibrium Green's functions. Although the expression for $I_{\rm L}$ includes $G^{r}_{11,\sigma}$ and $G^{<}_{11,\sigma}$, $G^{<}_{11,\sigma}$ is eliminated by making use of the conservation of total current. We finally obtain the current as

$$\begin{aligned} I &= \frac{e}{h} \sum_{\sigma} \int {\rm d}\omega T_{\sigma}(\omega)[f_{\rm L}(\omega) - f_{\rm R}(\omega)], \\ T_{\sigma}(\omega) &= \big[T_r + \sqrt{\alpha T_r(1-T_r)}\tilde{\Gamma}\cos\phi \, {\rm Re}\, G^{r}_{11,\sigma}(\omega) \\ &\quad - \tfrac{1}{2}[\alpha(1 - T_r\cos^2\phi) - T_r]\tilde{\Gamma}\, {\rm Im}\, G^{r}_{11,\sigma}(\omega)\big], \end{aligned} \tag{2.32}$$

where $T_{\sigma}(\omega)$ is the transmission probability and $\tilde{\Gamma} = \Gamma/(1+\xi)$. We use the above equation to calculate the differential conductance. Similarly, we obtain the current for $t_c \neq 0$.

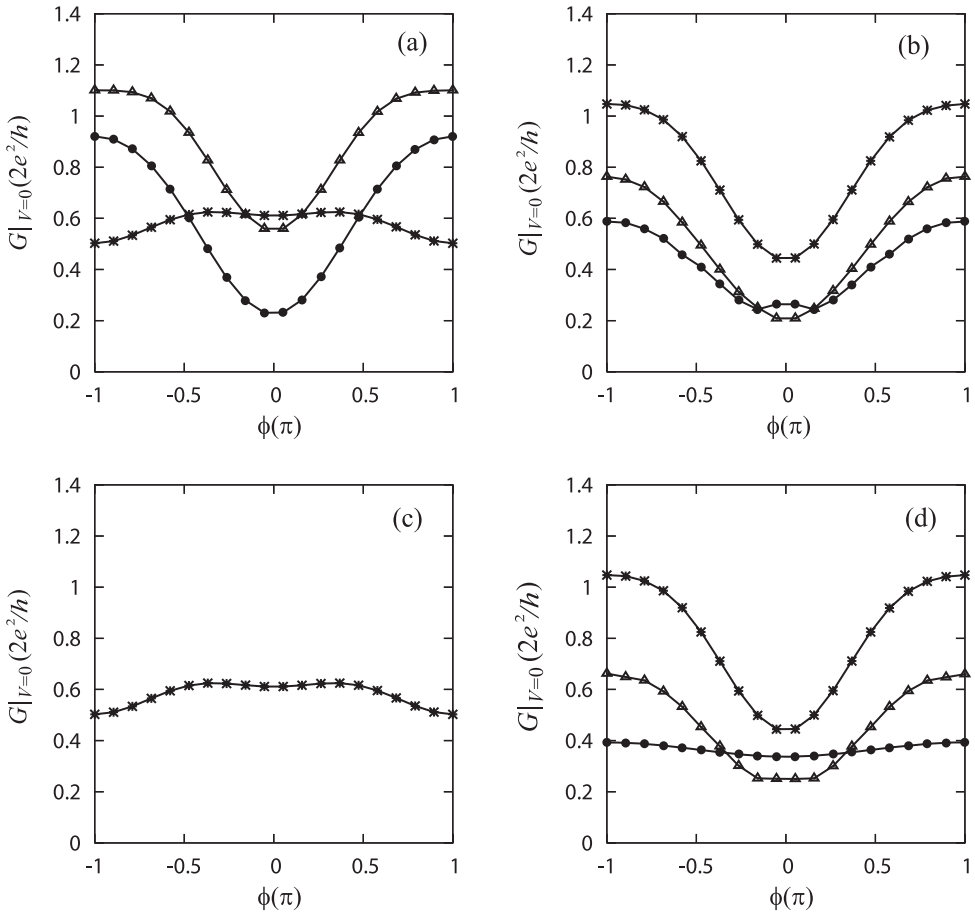

Figure 8. Dependence of the AB oscillation in zero-bias conductance on the energy levels of dots. $k_B T = 0.05$ and $\xi = 0.05$. (a) $t_c = 0.0$ and $\epsilon_2 = -3.0$. Curves denoted by $*$, $\triangle$, and $\bullet$ correspond to cases $\epsilon_1 = -2.0$, -1.0, and 0.0, respectively. (b) $t_c = 2.0$ and $\epsilon_2 = -3.0$. Curves denoted by $*$, $\triangle$, and $\bullet$ correspond to cases $\epsilon_1 = -2.0$, -1.0, and 0.0, respectively. (c) $t_c = 0.0$ and $\epsilon_1 = -2.0$. The curve denoted by $*$ does not depend on ϵ_2. (d) $t_c = 2.0$ and $\epsilon_1 = -2.0$. Curves denoted by $*$, $\triangle$, and $\bullet$ correspond to cases $\epsilon_2 = -3.0$, -1.5, and 0.0, respectively.

Because dot 2 is not connected with the leads, it turns out that the expression for current for the T-shaped DQD interferometer is the same as equation (2.32). It should be noted that $G^r_{11,\sigma}$ must be calculated in the presence of an infinitely large Coulomb interaction, and the effect of the direct tunneling between the leads must be taken into consideration. For this purpose, the following renormalized linewidth functions are used in the NCA calculation:

$$\tilde{\Gamma}^{\mathrm{L}}_{11} = \frac{\Gamma^{\mathrm{L}}_{11} + \xi\Gamma^{\mathrm{R}}_{11} - 2\sqrt{\xi\Gamma^{\mathrm{L}}_{11}\Gamma^{\mathrm{R}}_{11}}\sin\phi}{(1+\xi)^2},$$
$$\tilde{\Gamma}^{\mathrm{R}}_{11} = \frac{\Gamma^{\mathrm{R}}_{11} + \xi\Gamma^{\mathrm{L}}_{11} + 2\sqrt{\xi\Gamma^{\mathrm{L}}_{11}\Gamma^{\mathrm{R}}_{11}}\sin\phi}{(1+\xi)^2}. \tag{2.33}$$

The above renormalized linewidth functions were introduced by Kim and Hershfield [12]. They studied a quantum interferometer with a single dot under infinitely large Coulomb interaction. The self-energy for an electron in the Anderson impurity (dot 1) embedded in an effective electron continuum band was divided into one-body and many-body contributions. The first one corresponded to hopping into the continuum band, and the second one corresponded to the on-site Coulomb interaction. In their NCA scheme, the auxiliary Green's functions were introduced to describe the one-body contribution. For the lesser and greater self-energies of a quantum dot due to the hopping into leads, the bare linewidth functions $\Gamma^{\mathrm{L},(\mathrm{R})}_{11}$ were replaced by the renormalized linewidth functions $\tilde{\Gamma}^{\mathrm{L},(\mathrm{R})}_{11}$. The renormalized linewidth functions reflected the direct path between the leads, which were AB phase dependent. The NCA calculation for our T-shaped DQD interferometer is similar to that for their interferometer with a system with one embedded dot. The difference is that the interdot coupling is taken into consideration. We replace Γ^{L}_{11} and Γ^{R}_{11} by the renormalized ones and calculate $G_{11,\sigma}$ following the NCA scheme formulated in the previous subsection. Thus, the T-shaped DQD interferometer is converted into a T-shaped DQD system with phase-dependent linewidth functions. This causes asymmetric couplings between dot 1 and the leads even if $\alpha = 1.0$.

The parameters are almost same as those of the T-shaped DQD system in the previous subsection. $\Gamma = 1.0$ is fixed and all energies are scaled by Γ. The Kondo temperature is independent of ϕ, as shown in the previous subsection. The dependence of the AB oscillation on the energy levels of dots is shown in figure 8. As shown in figure 4(a), for a fixed ϵ_2 with a large t_c, there exists an optimal ϵ_1 for which the zero-bias conductance becomes maximum. When $t_c = 2.0$,

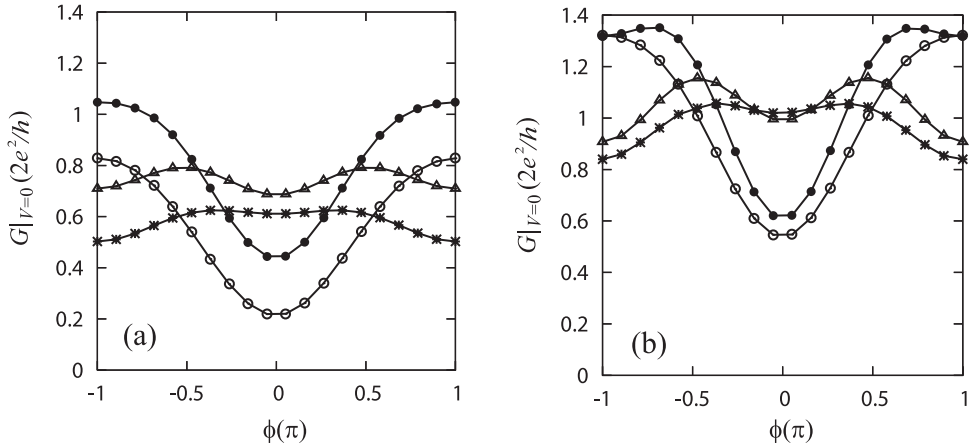

Figure 9. Dependence of the AB oscillation in zero-bias conductance on t_c. $k_BT = 0.05$, $\epsilon_1 = -2.0$, and $\epsilon_2 = -3.0$. Curves denoted by $*$, $\triangle$, $\bullet$, and $\circ$ correspond to cases $t_c = 0.0$, 1.5, 2.0, and 2.5, respectively. (a) $\xi = 0.05$ ($T_r = 0.18$) and (b) $\xi = 0.15$ ($T_r = 0.45$).

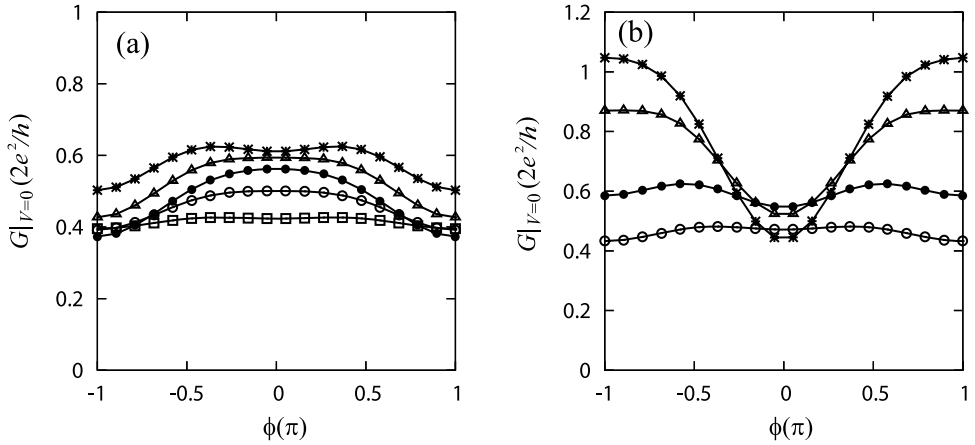

Figure 10. Dependence of AB oscillation in zero-bias conductance on temperature. $\epsilon_1 = -2.0$ and $\epsilon_2 = -3.0$. Curves denoted by $*$, $\triangle$, $\bullet$, $\circ$, and $\square$ correspond to cases $k_BT = 0.05$, 0.1, 0.3, 1.0, and 3.0, respectively. (a) $t_c = 0.0$ and (b) $t_c = 2.0$.

the zero-bias conductance is monotonically suppressed as $|\epsilon_1|$ decreases. These properties of the T-shaped DQD system result in the enhancement of the amplitude of the AB oscillation in the case of a large t_c with $\epsilon_1 = -2.0$. On the contrary, in the case of a large t_c with $\epsilon_1 = 0.0$, the AB oscillation is suppressed (compare figures 8(a) and (b)). For a fixed ϵ_1 with a large t_c, similar behavior is observed, as shown in figures 8(c) and (d).

In the following discussion, the energy levels of the dots are fixed at $\epsilon_1 = -2.0$ and $\epsilon_2 = -3.0$. The dependence of the AB oscillation in the zero-bias conductance on t_c is shown in figure 9. The zero-bias conductance is oscillatory, and its period is 2π. For a small t_c, the AB oscillation is small. However, for a large t_c, the AB oscillation increases and the zero-bias conductance is minimum at $\phi = 0$. In the previous subsection, the dependence of the zero-bias conductance on t_c in the absence of the magnetic field has been studied, and is shown in figure 2. For that case, the zero-bias conductance is determined by only Im $G^r_{11,\sigma}$ around the Fermi level. There is an optimal t_c for the zero-bias conductance in the range $1.5 < t_c < 2.5$. For the T-shaped DQD interferometer, the amplitude of the AB oscillation becomes significantly large for $t_c > 1.5$. The zero-bias conductance is determined by the transmission probability around the Fermi level by equation (2.32). This suggests that the real and imaginary parts of the retarded Green's function are combined through ϕ. The mechanism of the large AB oscillation for $t_c > 1.5$ results from the dependence of the zero-bias conductance on t_c of the T-shaped DQD system.

The dependence of the AB oscillation on temperature is shown in figure 10. As the temperature decreases, the AB oscillation becomes large. In particular, for $t_c = 2.0$, the amplitude becomes significantly large. When $t_c = 0$, at high temperatures a local spin in dot 1 acts as a scattering center for the conduction electrons, which reduces the flow of electrons via dot 1. As the temperature decreases, the spin in dot 1 forms the Kondo singlet state with the conduction electrons in the leads, and the electrons flow coherently via dot 1. Thus, the AB oscillation becomes large as temperature decreases. For optimal t_c ($\sim$2.0), the effective energy level ϵ_+ passes through the Fermi level, and the zero-bias conductance becomes large. This leads to a significantly large AB oscillation. In our calculation, the temperature is higher than the temperature in the study that employed the numerical renormalization group method [18]. As a result, the AB oscillation is a sinusoidal curve, and there are no higher harmonic components.

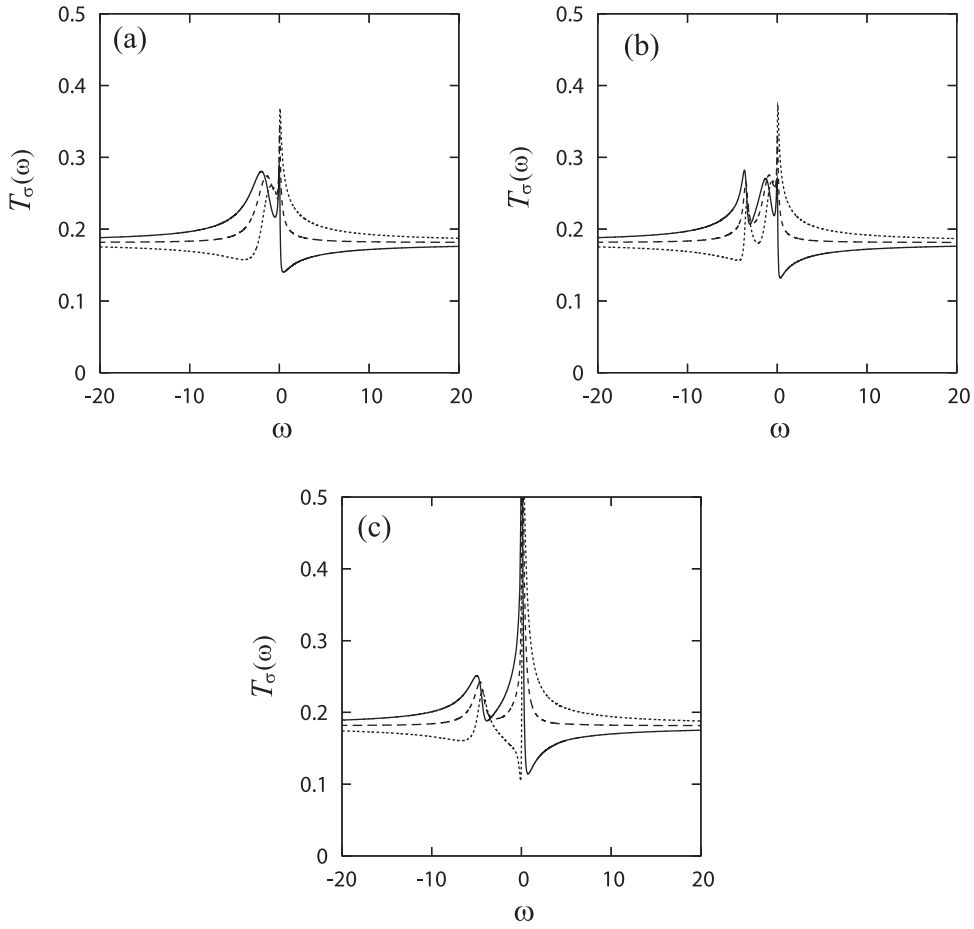

Figure 11. Transmission probability under zero-bias voltage. $k_B T = 0.05$, $\epsilon_1 = -2.0$, and $\epsilon_2 = -3.0$. Dotted, dashed and solid curves correspond to cases $\phi = 0.0, \pi/2$, and π, respectively. (a) $t_c = 0.0$, (b) $t_c = 1.0$, and (c) $t_c = 2.0$.

The transmission probability is shown in figure 11. Although $\alpha = 1.0$ in our calculations, it should be noted that the transmission probability for the case $\alpha \neq 1$ is qualitatively the same as that for $\alpha = 1$ [12]. It should be noted that each renormalized linewidth function is phase dependent; however, the sum is independent of the phase, $(\tilde{\Gamma}^{\rm L}_{11} + \tilde{\Gamma}^{\rm R}_{11}) = (\Gamma^{\rm L}_{11} + \Gamma^{\rm R}_{11})/(1+\xi) \equiv \tilde{\Gamma}$. In equilibrium, $f_{\rm L} = f_{\rm R}$, and $G^r_{11,\sigma}$ is invariant under the inversion of the AB phase $\phi \leftrightarrow -\phi$, i.e. $G^r_{11,\sigma}(\phi) = G^r_{11,\sigma}(-\phi)$. Owing to this AB phase symmetry of $G^r_{11,\sigma}$ and the periodicity of the transmission probability, it is sufficient to study the phase dependence of the transmission probability under zero-bias voltage in the range $0 \leqslant \phi \leqslant \pi$. We observe a dip and a peak, i.e. the Fano structure, except for the case $\phi = \pi/2$, as shown in figure 11. For a small t_c, the Kondo-related peak at $\omega = 0$ and a small peak corresponding to the bare energy level of dot 2 are observed. When $\phi = 0$, a dip and a peak are observed below and above the Fermi level, respectively. On the contrary, for $\phi = \pi$, a peak and a dip are observed below and above the Fermi level, respectively. For a large t_c, the Coulomb-related peak is split into two peaks located around the effective energy levels $\epsilon_\pm$. Although the positions of the peaks are shifted, the Fano structure still exists. When the electron path via dot 1 and the direct tunneling path between the leads interfere strongly, the Fano interference is enhanced in the transmission probability. The above condition is satisfied when t_c is around the optimal value for the zero-bias conductance and ξ ($\leqslant 1.0$) is large. For this case, the AB oscillation is large, as shown in figure 9.

The differential conductance under bias voltage and its blow-up in a small bias region are shown as in figures 12 and 13, respectively. Under finite bias, $f_{\rm L} \neq f_{\rm R}$, and the AB phase symmetry in $G^r_{11,\sigma}$ is broken, i.e. $G^r_{11,\sigma}(\phi) \neq G^r_{11,\sigma}(-\phi)$. The transmission probability and the differential conductance under the bias voltage do not have the AB phase symmetry. The asymmetry results from the ϕ dependence of the renormalized linewidth functions (equation (2.33)). It results in asymmetric coupling under a magnetic field even if $\Gamma^{\rm L}_{11} = \Gamma^{\rm R}_{11}$. For $t_c = 0$, the zero-bias conductance is small and the AB phase asymmetry is weak. Around the optimal t_c, the zero-bias conductance becomes large and the AB phase asymmetry in the differential conductance is also enhanced (compare cases $\phi = \pi/2$ and $-\pi/2$ in figure 13). The dependence of the linewidth function on ϕ causes the breakdown of the Onsager relation under finite voltage. It is shown that when the Onsager relation is broken in non-equilibrium, the nonlinear conductance becomes asymmetric under a magnetic field reversal [30]. This is due to the magnetic field dependence of the screening potential within a mesoscopic conductor.

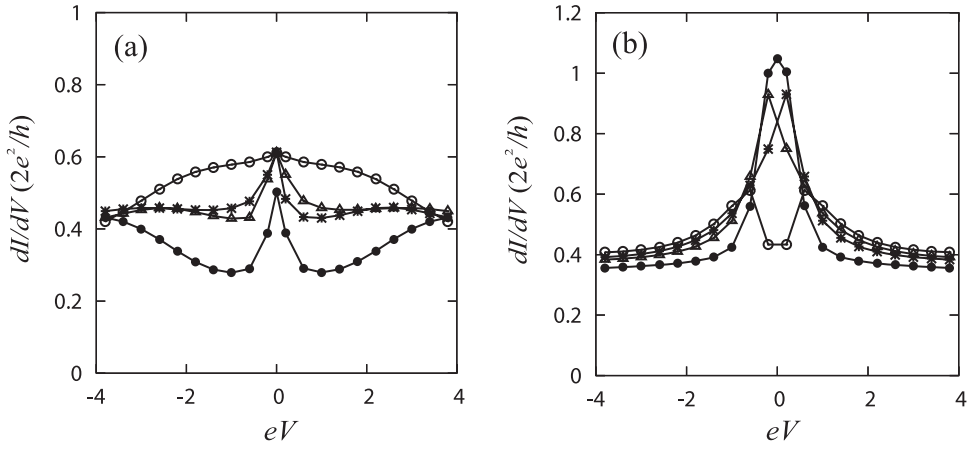

Figure 12. Differential conductance for different values of t_c. $k_BT = 0.05$, $\epsilon_1 = -2.0$, and $\epsilon_2 = -3.0$. Curves denoted by ○, ∗, △, and ● correspond to cases $\phi = 0, \pi/2, -\pi/2$, and π, respectively. (a) $t_c = 0.0$ and (b) $t_c = 2.0$.

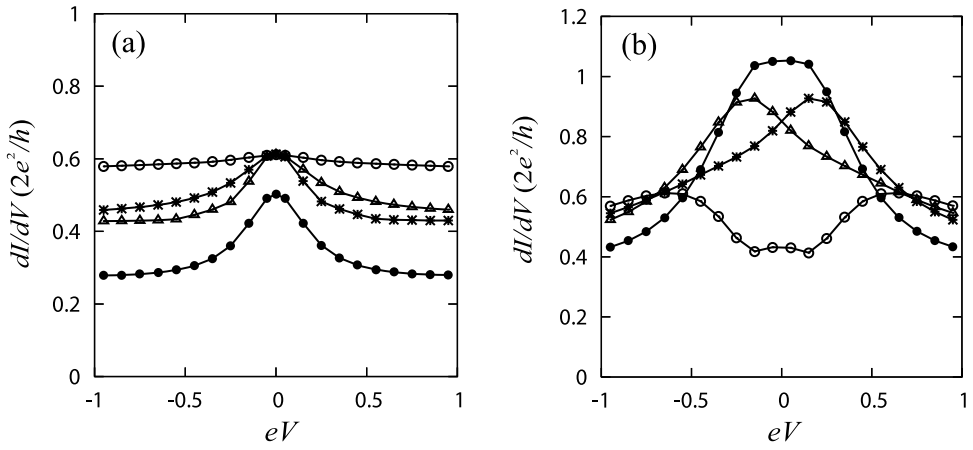

Figure 13. Blowup of differential conductance in small bias region. $k_BT = 0.05$. Curves denoted by ○, ∗, △, and ● correspond to cases $\phi = 0, \pi/2, -\pi/2$, and π, respectively. (a) $t_c = 0.0$ and (b) $t_c = 2.0$.

3. Conclusions

We have studied the conductance of a T-shaped DQD system under infinitely large Coulomb interaction.

First, we formulated the NCA scheme for the non-equilibrium states and studied the properties of the T-shaped DQD system in the absence of a magnetic field. In our calculation, the Kondo temperature is high, and the splitting of the Kondo peak does not appear in the DOS. The splitting of the zero-bias anomaly in the differential conductance and the optimal temperature in the zero-bias conductance indicate the quantum coherence between the two many-body Kondo states on each dot [23]. However, these are observed at significantly low temperatures. In our calculation, the Coulomb peak splits in the DOS as t_c increases, and there is an optimal t_c for the zero-bias conductance. The existence of the optimal t_c causes the non-monotonic behavior in the differential conductance and the temperature dependence of the zero-bias conductance.

Second, we applied the above mentioned NCA scheme to a T-shaped DQD interferometer. In the quantum interferometer, there is a direct tunneling path between the leads. In order to assimilate the effect of the direct tunneling path into the NCA scheme, we replaced the linewidth functions with the renormalized ones. This replacement converted the T-shaped DQD interferometer into a T-shaped DQD system with the AB phase-dependent couplings. The zero-bias conductance is AB phase symmetric. However, the AB phase symmetry is broken under finite bias, and the asymmetry is enhanced as t_c increased. The AB oscillation in the zero-bias conductance is large at the optimal t_c, which is determined in the T-shaped DQD system. The AB oscillation in the zero-bias conductance depended on t_c, temperature, and ξ. The existence of the optimal t_c is specific to the T-shaped DQD interferometer. From the above results, we deduced the properties of the T-shaped DQD interferometer used in the experiment; the Kondo temperature is high, the AB oscillation becomes large at an optimal t_c, and the differential conductance is asymmetric with respect to $V = 0$.

Acknowledgments

The author would like to thank Dr Y Tokura, Dr Y Imai, and Dr R Sakano for their valuable discussions and comments.

References

[1] Tanaka Y and Kawakami N 2005 *Phys. Rev.* B **72** 085304
[2] López R, Sánchez D and Serra L 2007 *Phys. Rev.* B **76** 035307
[3] Tarucha S, Austing D G, Honda T, van der Hage R J and Kouwenhoven L P 1996 *Phys. Rev. Lett.* **77** 3613
[4] van der Wiel W G, De Franceschi S, Elzerman J M, Fujisawa T, Tarucha S and Kouwenhoven L P 2003 *Rev. Mod. Phys.* **75** 1
[5] Hüttel A K, Ludwig S, Lorenz H, Eberl K and Kotthaus J P 2005 *Phys. Rev.* B **72** 081310(R)
[6] Hewson A C 1997 *The Kondo Problem to Heavy Fermions* (*Cambridge Studies in Magnetism*) (Cambridge: Cambridge University Press)
[7] Izumida W and Sakai O 2005 *J. Phys. Soc. Japan* **74** 103
[8] Izumida W and Sakai O 2000 *Phys. Rev.* B **62** 10260
[9] Cornaglia P S and Grempel D R 2005 *Phys. Rev.* B **71** 075305
[10] Takazawa Y, Imai Y and Kawakami N 2002 *J. Phys. Soc. Japan* **71** 2234
[11] Ueda A and Eto M 2006 *Phys. Rev.* B **73** 235353
[12] Kim T-S and Hershfield S 2003 *Phys. Rev.* B **67** 165313
[13] Akera H 1993 *Phys. Rev.* B **47** 6835
[14] Hofstetter W, König J and Schoeller H 2001 *Phys. Rev. Lett.* **87** 156803
[15] König J and Gefen Y 2002 *Phys. Rev.* B **65** 045316
[16] Kobayashi K, Aikawa H, Katsumoto S and Iye Y 2002 *Phys. Rev. Lett.* **88** 256806
[17] Aikawa H, Kobayashi K, Sano A, Katsumoto S and Iye Y 2004 *Phys. Rev. Lett.* **92** 176802
[18] Izumida W, Sakai O and Shimizu Y 1997 *J. Phys. Soc. Japan* **66** 717
[19] Pruschke Th and Grewe N 1989 *Z. Phys.* B **74** 439
[20] Hettler M, Kroha J and Hershfield S 1998 *Phys. Rev.* B **58** 5649
[21] Jauho A P, Wingreen N S and Meir Y 1994 *Phys. Rev.* B **50** 5528
[22] Meir Y and Wingreen N S 1992 *Phys. Rev. Lett.* **68** 2512
[23] Aguado R and Langreth D C 2003 *Phys. Rev.* B **67** 245307
[24] Georges A and Meir Y 1999 *Phys. Rev. Lett.* **82** 3508
[25] Aono T and Eto M 2001 *Phys. Rev.* B **63** 125327
[26] Aono T, Eto M and Kawamura K 1998 *J. Phys. Soc. Japan* **67** 1860
[27] Tanaka Y and Kawakami N 2004 *J. Phys. Soc. Japan* **73** 2795
[28] Aguado R and Langreth D C 2000 *Phys. Rev. Lett.* **85** 1946
[29] López R, Aguado R and Platero G 2002 *Phys. Rev. Lett.* **89** 136802
[30] Sánchez D and Büttiker M 2004 *Phys. Rev. Lett.* **93** 106802